This is a self-archived – parallel published version of an original article. This version may differ from the original in pagination and typographic details. When using please cite the original.

Self-Synthesizing Nanorods from Dynamic Combinatorial Libraries against Drug Resistant Cancer

Yu Cao[a][II], Jian Yang[b,c][II], Dominik Eichin[a], Fangzhe Zhao[b,c], Dawei Qi[a], Laura Kahari[a], Chunman Jia[d], Markus Peurla[e], Jessica M. Rosenholm[f], Zhao Zhao[a], Sirpa Jalkanen[a], Jianwei Li [a,d]*

[a] Dr. Yu Cao, Dominik Eichin, Dawei Qi, Laura Kahari, Zhao Zhao, Prof. Sirpa Jalkanen, Dr. Jianwei Li
MediCity Research Laboratory
University of Turku
Tykistökatu 6, FI-20520 Turku, Finland
E-mail: jianwei.li@utu.fi

[b] Dr. Jian Yang, Fangzhe Zhao
State Key Laboratory of Component-based Chinese Medicine
Tianjin International Joint Academy of Biotechnology & Medicine
Tianjin, P.R. China

[c] Dr. Jian Yang, Fangzhe Zhao
Research and Development Center of Tianjin University of Traditional Chinese Medicine
Tianjin International Joint Academy of Biotechnology & Medicine
Tianjin, P.R. China

[d] Prof. Chunman Jia, Dr. Jianwei Li
Hainan Provincial Key Lab of Fine Chem, Key laboratory of Advanced Materials of Tropical Island Resources of Ministry of Education
Hainan University
Haikou 570228, P.R. China
E-mail: jianwei.li@utu.fi

[e] Markus Peurla
Institute of Biomedicine and FICAN West Cancer Research Laboratories
University of Turku
Kiinamyllynkatu 10, FI-20520 Turku, Finland

[f] Prof. Jessica M. Rosenholm
Pharmaceutical Sciences Laboratory, Faculty of Science and Engineering
Åbo Akademi University
Tykistökatu 6, FI-20520 Turku, Finland

[II] These authors contributed equally to this work.

Abstract: Molecular self-assembly has been widely used to develop nanocarriers for drug delivery; however, most have unsatisfactory drug loading capacity (DLC) and the dilemma between stimuli-responsiveness and stability, stagnating their translational process. Here we overcame these drawbacks using dynamic combinatorial chemistry. A carrier molecule was spontaneously and quantitatively synthesized, aided by co-self-assembly with a template molecule and an anti-cancer drug doxorubicin (DOX) from a dynamic combinatorial library that was operated by disulfide exchange under thermodynamic control. The highly selective synthesis guaranteed a stable yet pH- and redox- responsive nanocarrier with a maximized DLC of 40.1% and an enhanced drug potency to fight DOX resistance *in vitro* and *in vivo*. Our findings suggested that harnessing the interplay between synthesis and self-assembly in complex chemical systems could yield functional nanomaterials for advanced applications.

Introduction

Molecular self-assembly is a powerful nanotechnology used to develop nanocarriers that deliver anti-cancer drugs to tumour sites for chemotherapy.[1] For this purpose, nanocarriers are usually self-assembled by amphiphilic molecules through non-covalent interactions and drug molecules are encapsulated in the nanocarriers.[2] Nanocarriers with tailored properties not only pro-tect the inclusive drugs from degradation and promote drug bio-availability, but also selectively deliver drugs to tumour lesions via the enhanced permeation and retention (EPR) effect.[3] An ideal nanomaterial for drug delivery has a high drug-loading capacity and is stable while it is transported to cancer cells but can also release drug molecules at tumour sites.[4]

It has been a challenge to explore nanocarriers for drug delivery possessing all these merits simultaneously. Significant efforts have been made to develop various self-assembling molecules, such as liposomes,[5] linear/miktoarm polymers[6] and dendrimers.[7] Though some materials have been available for clinical anti-cancer treatment, most commercialized products suffer from low drug-loading degrees (generally less than 10%) and usually disassemble easily during the delivery process.[8] Apart from these traditional self-assembling molecules, self-assembling prodrugs have received recent attention as a promising strategy to enhance drug-loading contents for drug delivery.[9] However, prodrugs still face many long-standing challenges including their insolubility, toxicity and poor bioavailability and pharmacokinetics.[10] These drawbacks have been attributed to the inherent disadvantages of current design strategies for the material. Normally, the traditional self-assemblers and the prodrugs are screened out from many candidate molecules. This process is time-consuming, as it requires tedious design, synthesis and testing. [1a] In contrast, nature often produces functional molecules at a systems level rather than through an inefficient step-by-step process. Molecules in living systems evolve intelligently

by responding to and adapting to changes in the natural environment. Natural selection integrates error correction into synthesis, enabling selected molecules to fit their operating systems perfectly.[11] We have proposed that imitating nature and finding a spontaneous synthesis strategy at a system level will create nanocarrier molecules effective for drug delivery.

Dynamic combinatorial chemistry (DCC) possesses a synthesis principle akin to that found in nature.[12] It deals with dynamic combinatorial libraries (DCLs), which are pools of interconverting molecules that exchange building blocks *via* reversible chemical reactions. The concentration distribution of library members is typically under thermodynamic equilibrium. The introduction of an external stimulus, for example, template molecules capable of binding tightly to a library member, lowers the energy level of the target library member and shifts the equilibrium of the mixture towards the library member's concentration amplification. Researchers have used this working principle to show that DCC is a powerful strategy for exploring synthetic receptors for biomacromolecules,[13] complex interlocked structures,[14] dynamic catalysts[15] and self-replicating molecules[16]. We are among the

nanocarriers for drug delivery. When a library species is amplified by a template molecule, matched binding gives rise to a supramolecular complex. If the complex can aggregate and self-assemble with drug molecules, then a secondary thermodynamic control process will assist the synthesis of the target library member, producing co-self-assembled nanocarriers with encapsulated drug molecules. Thus, co-self-assembly directs the system to synthesize the very self-assembling molecules spontaneously. The resulting nanomaterials are known as self-synthesizing nanocarriers. A DCC-based self-synthesizing strategy has several advantages for drug delivery. First, the synthesis of the nanocarrier molecule is highly selected by the drug molecule, which ensures a relatively strong association between the nanocarrier and drug molecules. This enhances drug-loading capacity. Furthermore, spontaneous synthesis under thermodynamic control produces relatively stable co-self-assembled nanostructures. Finally, the reversible nature of chemical reactions for DCC will enable the nanomaterial responsive to release the encapsulated drug molecules when external stimuli are applied.
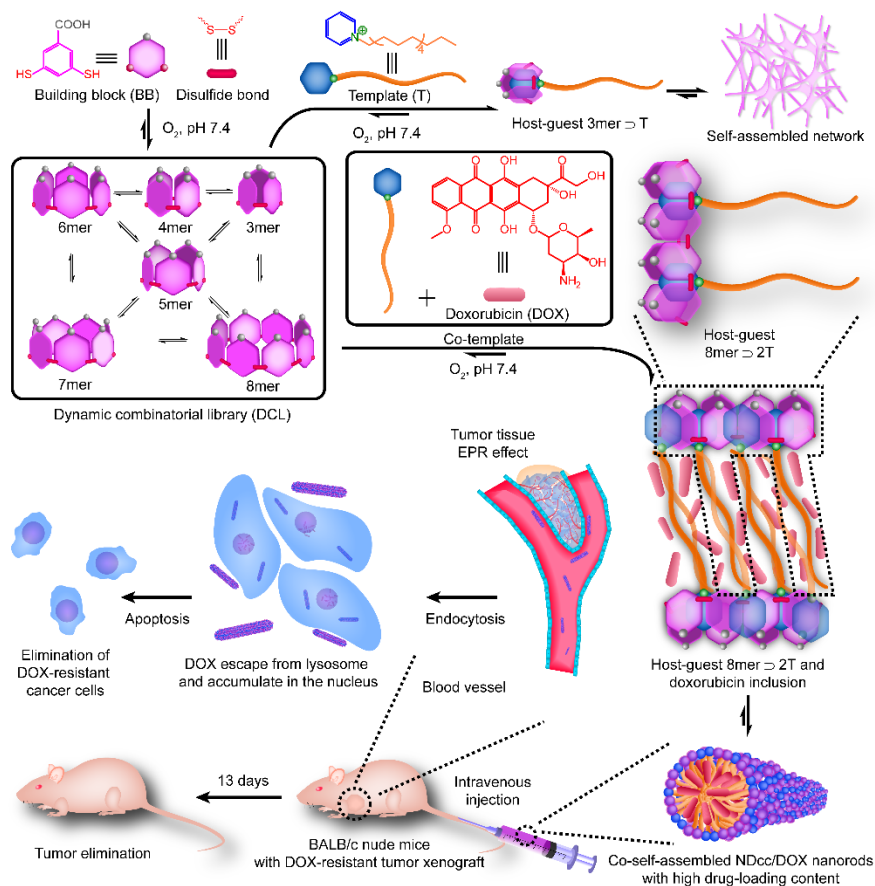
few who have suggested that it may also contribute to seeking

Scheme 1. Schematic illustration of self-synthesizing nanorods emerging from DCLs against DOX resistant cancer in *vitro* and in *vivo*. A dithiol building block (**BB**) could be oxidized in the air to generate a DCL of potential disulfide macrocycles with various sizes under pH 7.4 at 298 K. With the addition of a pyridine template (**T**), the trimer (3mer) was the dominated species due to the formation of an amphiphilic complex 3mer ⊃ **T** that further self-assembled into nanofiber-based network structures. When a hydrophobic anticancer drug doxorubicin (DOX) and the **T** were both introduced into the same library, an octamer (8mer) instead of the 3mer was quantitatively amplified. The amplification mechanism was similar to that of the 3mer. The outcome of the self-synthesizing strategy driven by co-self-assembly were rigid nanorods. Upon introduction of the DOX molecule, the hydrophobic drug was encapsulated into the hydrophobic domain of the self-synthesizing nanorods. The resulting nanomaterials could overcome DOX resistance *in vitro* and *in vivo*.

In this study, we mimicked nature selection using DCC to explore self-synthesizing nanocarriers with high drug-loading contents that are stable yet dual-responsive for anti-cancer drug delivery (Scheme 1). After the introduction of a template and drug molecule into a DCL prepared from a dithiol building block, the fittest octameric disulfide macrocyclic molecule (8mer) was quantitatively amplified under a thermodynamic selection. The selected macrocycle minimized the energy level of the complex system, and the formation of the right molecule 8mer, during the co-self-assembly process, aided the encapsulation of a drug molecule doxorubicin (DOX) with a very high drug-loading content (40.1%). The resulting nanorods had a low energy level, so they were stable enough to enhance drug accumulation and anti-tumour potency *via* nano-formulation. Furthermore, the redox- and pH-responsive nature of the disulfide-linked macrocycle with carboxylic acids allowed the nanorods to release drug molecules inside the tumour cells. Finally, the smart nanorods showed a powerful ability to fight DOX-resistant cancer both *in vitro* and *in vivo*. These findings suggested that, from a systems chemistry perspective, the interplay between synthesis and self-assembly in complex chemical systems is a powerful workhorse giving rise to self-synthesizing materials. This has opened up a new path for exploring drug delivery carriers and has provided a promising and effective tool for cancer chemotherapy.

Results and Discussion

Macrocyclic receptors linked by disulfide bonds can be amplified by template molecules through their binding in DCLs.[17] If the resulting complex is a supra-amphiphile, then subsequent co-self-assembly will take place. Guided by this hypothesis, we chose a well-studied dithiol building block **BB** functionalized with a carboxylic acid group, and we designed a cationic molecule with a long aliphatic tail as a template molecule **T**. The carboxylic acid group of the building block could be deprotonated at physiological pH, making it water-soluble and providing the oxidized macrocycles with negative charges, which have a potential association with the pyridinium cation group of the template **T**. In addition, the aliphatic tail of the template owning a hydrophobic property could make the resulting complex amphiphilic. An anti-cancer drug DOX was selected as a model drug that is poorly water-soluble at physiological conditions, meaning that it could be buried in the hydrophobic domain of co-self-assembled nanomaterials.

As before,[18] we prepared a DCL from the building block **BB**, at a concentration of 1.88 mM in a phosphate-buffered saline (PBS) buffer (pH 7.4). The library was vigorously stirred and fully oxidized in the air after 7 days. High performance liquid chromatography–mass spectrometry (HPLC-MS) analysis showed that the main species were the trimer (3mer) and tetramer (4mer) of the building block **BB** (Fig. 1a). When the building block **BB** (1.88 mM) and DOX (0.87 mM) were used for a library, DOX could not be dissolved during the whole oxidation process. The final concentration distribution of the two species (3mer and 4mer) was the same as in the library prepared only from the building block **BB** (Fig. 1b). However, in a parallel library (the NDcc library) made from the building block **BB** (1.88 mM) and the template **T** (0.94 mM), the dominant species was the 3mer while the 4mer nearly disappeared (Fig.1c). Thus, the drug alone gave no amplification effect to the library, but the template **T** amplified the 3mer.
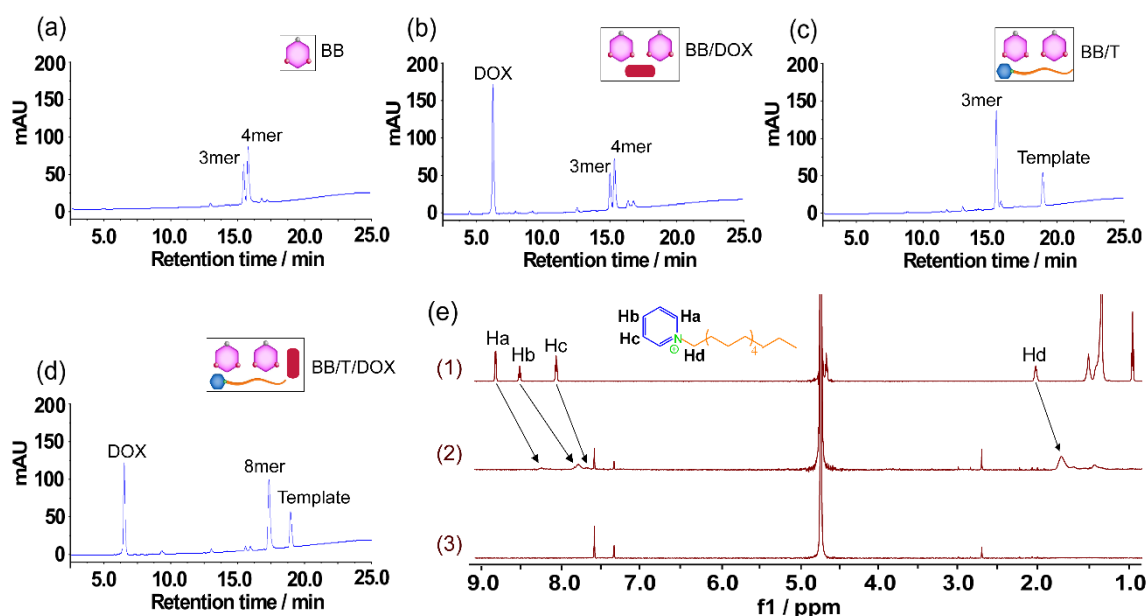

Figure 1. Component and molecular association analysis of dynamic BB/T/Drug combinatorial systems. HPLC analysis at 254 nm of DCLs oxidized after 1 week at pH 7.4 at room temperature: the DCL prepared from (a) **BB** alone (1.88 mM); (b) **BB** (1.88 mM) and DOX (0.87 mM); (c) **BB** (1.88 mM) and **T** (0.94 mM); (d) **BB** (1.88 mM), **T** (0.94 mM) and DOX (0.87 mM). (e) ^{1}H NMR (600 MHz) analysis of samples made from (1) the template **T** alone (1 mM), (2) the template **T** (1 mM) and 8mer (0.2 mM) and (3) 8mer alone (0.2 mM). The spectra were recorded at 298 K in 10 mM phosphate buffer (pD 7.4, 11% D$_2$O) with water presaturation.

To test the feasibility of exploring nanomaterials using DCC at a systems level, we introduced the template **T** and DOX together at the same time in a single library (the NDcc/DOX library). Unlike precipitants in the library mixed by the **BB** and DOX, the NDcc/DOX library remained a clear red solution for longer than 2 months. Unexpectedly, a new species the 8mer of **BB** was almost quantitatively yielded (Fig. 1d). We had not observed this 8mer in any of the previous libraries. Such remarkable amplification could be re-formed by the partial reduction and reoxidation procedures, suggesting that the 8mer was a thermodynamic product.[19,20] In general, compared to the 3mer and 4mer, the 8mer was thermodynamically unfavored. However, the 8mer was amplified at the expense of macrocycles of other sizes when the template **T** and DOX were added. We attributed this size-selective amplification to the downhill co-self-assembly of the three constitutes.

To elucidate the molecular organization of the nanostructures emerging from the NDcc/DOX ternary library, we purified the 8mer using preparative HPLC and investigated its complexation with the template **T** using proton nuclear magnetic resonance (^{1}H NMR) spectroscopy. Upon the addition of the 8mer into a solution of the template **T** in D_2O (1 mM, pD 7.4), the signals of the pyridine protons (H_a, H_b and H_c) and the methylene protons H_d of the template **T** showed remarkable upfield shifts, owing to the shielding effect of the electron-rich cavities of the 8mer toward the template (Fig. 1e). These results revealed that the 8mer was fully threaded by the guest template with the H_a, H_b, H_c and H_d protons in the hydrophobic cavity of the 8mer. We also conducted two-dimensional nuclear overhauser effect (2D NOESY) experiments to study the spatial conformation of the inclusion complex (Fig. S4). The Nuclear Overhauser effect (NOE) correlation signals were observed between H_1 and H_2 protons on the 8mer and the

H_c pyridine protons on the template, confirming the above threading binding mode. Then, we used the Job's plot method on a UV−Vis spectrophotometer to show that the complex stoichiometry between the 8mer and the template **T** was 1:2 (Fig. S5 and Fig. S6). The binding constant (K_a) of the formation of the 8mer ⊃ 2**T** complex was further determined as 7.5 ×10^8 M^{-1} (Fig. S7 and Fig. S8) using UV-vis titration.

To investigate morphology in the complex system, we first examined a solution of only the template **T** (0.94 mM) under physiological conditions using transmission electron microscopy (TEM). Micelles with sizes around 32 nm were observed (see Fig. S9a). The ζ-potential of the same solution was determined as +22.4 mV using dynamic light scattering (Fig.2a). This highly positive ζ-potential suggested that strong repulsive forces existed between the pyridine moieties of the template **T**, which could prevent two molecular template **T** from being close enough to amplify 8mer. Instead, 3mer was amplified in the NDcc library by a single molecule of template **T**. We also prepared a solution of the template **T** (0.94 mM) and DOX with a target concentration of 0.87 mM. However, most DOX was not dissolved well. The morphology of the clear solution from this mixture was analysed using TEM. We observed micelles with larger sizes (around 57 nm) (see Fig. S9b), indicating the encapsulation of DOX into the hydrophobic domain of the micelles self-assembled by **T**. Interestingly, the ζ-potential of DOX encapsulated micelles was reduced to +10.0 mV (Fig.2a), which allowed two molecular template **T** to work together for the amplification of 8mer in the NDcc/DOX library.

As the 8mer ⊃ 2**T** complex was amphiphilic, it might have been able to form higher-order aggregates under physiological conditions. Its aggregation behavior was studied using TEM. We observed nanorods with a mean dimension of 25 nm × 250 nm in

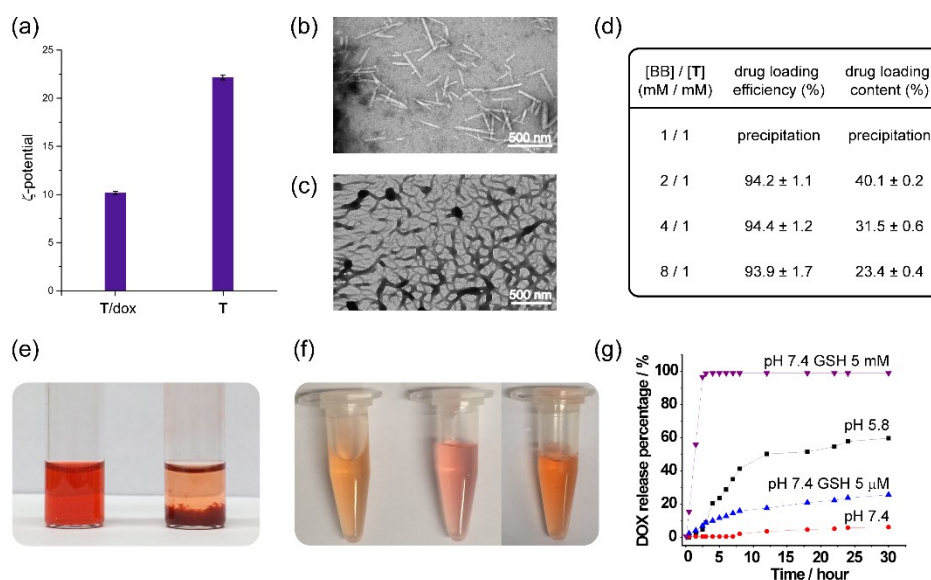| [BB] / [T] (mM / mM)	drug loading efficiency (%)	drug loading content (%)
1 / 1	precipitation	precipitation
2 / 1	94.2 ± 1.1	40.1 ± 0.2
4 / 1	94.4 ± 1.2	31.5 ± 0.6
8 / 1	93.9 ± 1.7	23.4 ± 0.4

Figure 2. (a) Zeta potential of a solution of only the template **T** (0.94 mM, pH 7.4) and a clear solution from the mixture of the template **T** (0.94 mM) and DOX (target concentration: 0.87 mM, pH 7.4); TEM micrographs of nanostructures from the (b) NDcc/DOX and (c) NDcc library. (d) Screening the ratios of building block **BB** and template **T** for the optimal drug-loading contents. (e) Visual comparison photos between NDcc/DOX library (left) and DOX alone (right) at pH 7.4. (f) Visual comparison pictures of NDcc/DOX nanorods (diluted 30 times) with addition of GSH 5 mM (left) at pH 7.4 (middle) and pH 5.8 (right). (g) Time course of DOX released from nanorods of the NDcc/DOX library at pH 5.8, pH 7.4, GSH 5 μM and GSH 5 mM at 37 °C.

fully oxidized NDcc/DOX libraries (Fig. 2b). Previous studies suggested that such a high aspect ratio may be particularly beneficial for drug delivery in cancer therapy, because this prevents the excretion of the drug by the kidneys and its sequestration in the spleen. In addition, due to their anisotropic properties, rod-shaped nanoparticles enhance internalization efficiency compared to spherical nanoparticles.[21-23] However, the size and morphology of nanostructures in the NDcc library varied. Without the introduction of DOX, aggregates in the NDcc library had a network structure (Fig. 2c). To understand how the three molecules were packed into nanorods, we analysed the HPLC spectra again. The Fig. 1(d) revealed that there were only peaks of the template **T**, the drug molecule DOX and 8mer. No additional peaks were observed, suggesting that the DOX did not covalently reacted with neither the template **T** nor the building block **BB**. Thus, the DOX should be physically encapsulated into the nanorods. The comparison between Fig.1(a) and Fig.1(b) indicated that DOX did not amplify any library species, so it did not bind with any disulfide macrocycles. Thereby, considering DOX is hydrophobic at pH 7.4, it should associate with the hydrophobic tails of the template **T**. Then, we checked the ^{1}H NMR spectrum of the sample prepared from DOX (1 mM), the 8mer (0.2 mM) and the template **T** (1 mM) (Fig. S10). The signal peaks of DOX were almost shielded and could not be clearly observed. This shielding effect suggested that DOX molecules were encapsulated in the inner part of the nanorods. The TEM analysis of the NDcc/DOX library (Fig. 2b) did not show any micelles self-assembled by solely template **T**. Furthermore, the overall concentration (0.94 mM) of the template **T** was higher than that (0.47 mM) involved in the binding with 8mer (0.24 mM) in the library. These results showed that the poorly water-soluble DOX was within the hydrophobic space co-assembled by 8mer ⊃ 2**T** complex and un-complexed template **T**. The co-self-assembly was mainly driven by hydrophobic interactions of alkyl chains of the un-complexed template **T** and the 8mer ⊃ 2**T** complex, which induced a preferred or spontaneous curvature of nanorods. Detailed molecular packing has been shown in the **Scheme 1**.
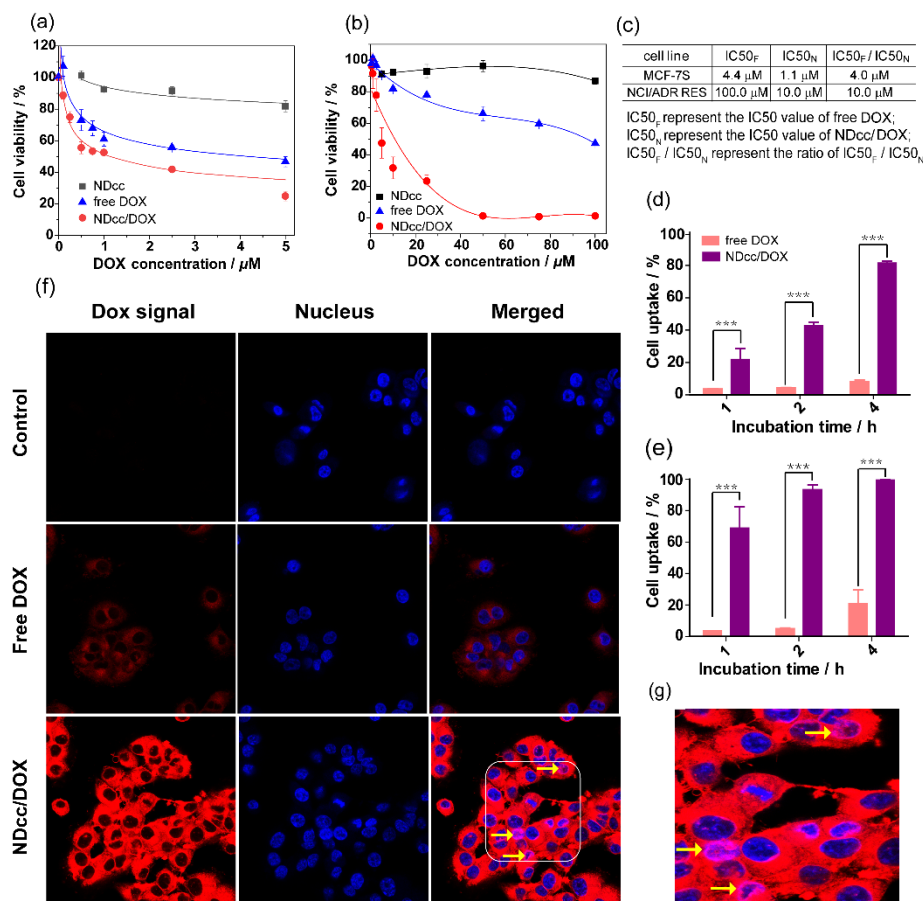

Figure 3. NDcc/DOX nanorods show enhanced antiproliferation efficiency via rapid, effective cellular uptake and inhibition of drug efflux. The antiproliferative activity of free DOX and NDcc/DOX nanorods on (a) drug-sensitive breast cancer MCF-7S cells and (b) drug-resistant NCI/RES-ADR cells were measured by cell counting kit-8 (CCK-8) assay. (c) The IC50 values of free DOX and NDcc/DOX nanorods were estimated and shown in this table. (d) The cellular uptake in drug-resistant NCI/RES-ADR cells was quantified using flow cytometry after treatment with free DOX (C_{dox} = 7.5 μM) and NDcc/DOX (C_{dox} = 7.5 μM) at 1 h, 2 h and 4 h. (e) The cellular uptake in drug-resistant NCI/RES-ADR cells was quantified using flow cytometry after treatment with free DOX (C_{dox} = 15 μM) and NDcc/DOX (C_{dox} = 15 μM) at 1 h, 2 h and 4 h. (f) The cellular uptake was imaged using confocal microscope following treatment with free DOX (C_{dox} = 15 μM) and NDcc/DOX (C_{dox} = 15 μM) at 8 h in NCI/RES-ADR cells. (Scale bar: 4 μm.) (g) The enlarge part of the white square in the cellular uptake image (f).

We continue to optimize the library condition for a maximum drug-loading content by changing the molar ratio among the building block **BB**, template **T** and DOX. Experimental details have been shown on page S2 of the Supporting Information. The maximum drug-loading capacity could be attained up to 40.1% and the corresponding encapsulation efficiency value was 94.2% (Fig. 2c). This high drug-loading content was primarily due to the spontaneous and highly selective synthesis of the 8mer driven by the co-self-assembly process. The self-synthesis of the right macrocycle could further adjust the size of the hydrophobic space to accommodate considerable drug payloads.

Altogether, the morphology, long-term stability and the high drug-loading capacity of the self-synthesizing nanorod suggested that it could be an ideal nanomaterial for efficient drug delivery.

Nanocarriers for cancer therapy must control the release profile of the therapeutic agent at tumour lesions. Changing the microenvironment within and outside cancer cells could trigger the responsiveness of nanocarriers to release drug molecules at tumour sites. Tumour lesions are usually more acidic (pH 5.5) than normal tissues due to the presence of excessive lactic acid and CO_2 as metabolites in a hypoxic microenvironment.[21] In addition, the concentration of glutathione (GSH) inside cancer cells (higher than 5 mM) is much higher than that in extracellular matrices (approximately 5 μM) at tumour sites.[22] These pH and redox conditions could control drug release from NDcc/DOX nanorods. Further investigation of the dual-responsiveness of the nanomaterials has been shown below.

As shown in Fig. 2e, NDcc/DOX nanorods in the pH 7.4 PBS buffer was a clear red solution, while the same amounts of DOX in the nanorods could not be dissolved well. To have a better visual observation, the nanorod solution (pH 7.4) was diluted 30 times and it appeared pink (Fig. 2f). With the introduction of GSH 5 mM or the adjustment of pH from 7.4 to 5.8, the solution turned orange (Fig. 2f) and the fluorescence intensity of the typical DOX peak increased over time (Fig. S11), indicating that DOX was released. Moreover, a gradual release of DOX was monitored by using HPLC under acidic conditions (pH 5.8) *in vitro*. Cumulatively, about 60% of the total DOX molecules in the nanorods were released in the first 30 h at pH 5.8, while there was a cumulative leakage of less than 5% within the same time period at pH 7.4 (Fig. 2g). Under physiological conditions, the carboxylic acid groups of the 8mer were deprotonated, which created an electrostatic interaction with the positive charge of the template **T**, keeping the nanostructure stable. When the pH became acidic (pH 5.8), the carboxylate anions of the 8mer were protonated again and the electrostatic interaction weakened, making the entire nano-entity fragile, which resulted in the release of the drug. The loaded amine-bearing DOX was more positively charged at pH 5.8 than at pH 7.4, which contributed to extra electrostatic repulsion between the drug DOX and the template **T**, further promoting drug release.

NDcc/DOX nanorods were reduction responsive. As shown in Fig. 2g, *in vitro* DOX release experiments revealed that drug release from nanorods at C_{GSH} 5 mM was more rapid and efficient than that at C_{GSH} 5 μM. A cumulative release of approximately 20% of DOX molecules was observed in the presence of 5 μM

GSH after incubating for 30 h, suggesting that minimal drug leakage would occur during blood circulation. Upon incubation for 2.5 h in the presence of 5 mM GSH, a cumulative drug release of 100% was achieved. These acid- and reduction- responsive drug release features endowed self-synthesizing nanorods with a preferential drug release profile, allowing them to release drug molecules at the tumour site rather than in normal tissues under physiological conditions.

After establishing the favourable drug release profile of NDcc/DOX nanorods, we evaluated their anti-proliferation efficiency in two types of cancer cell lines, MCF-7S DOX-sensitive human breast cancer cells and NCI/RES-ADR DOX-resistant human ovarian cancer cells.[24] As shown in Fig. 3a-c, the IC_{50} value of free DOX for NCI/RES-ADR cells was 100 μM while that for MCF-7S cells was only 4.4 μM. Such a strong resistance to DOX was attributed to the over-expression of P-glycoprotein (P-gp) by NCI/RES-ADR cells, as the P-gp pumped DOX molecules out of cancer cells.[25] DOX resistance could be overcome by nanocarriers that inhibit P-gp efflux and deplete adenosine triphosphate (ATP).[26] The IC_{50} value of NDcc/DOX nanorods for NCI/RES-ADR cells was 10 μM, suggesting a 10-fold toxicity of free DOX (Fig. 3c). NDcc/DOX nanorods could kill MCF-7S cancer cells even more efficiently by showing a lower IC_{50} value (1.1 μM). These results demonstrated that NDcc/DOX nanorods were considerably more efficient than free DOX in improving cell antiproliferation in both drug-sensitive and drug-resistant cell lines.

To understand the mechanism underlying the enhanced proliferation inhibition of NDcc/DOX nanorods, their cellular uptake was inspected in MCF-7S and NCI/RES-ADR cells using flow cytometry analysis. The drug uptake efficiencies of NCI/RES-ADR cells were approximately 10% and 25% when incubated with free DOX 7.5 μM and 15 μM for 4 h, respectively (Fig. 3d, Fig. 3e). In contrast, drug uptake was almost 100% after incubation for 2 h with NDcc/DOX nanorods (15 μM) (Fig. 3e), which suggested that DOX-loaded nanorods promoted the cellular internalization and accumulation of DOX in a time- and dose-dependent manner (Fig. 3d, Fig. 3e, Fig. 3f, Fig. S12a and Fig. S12b). The enhanced cellular uptake of NDcc/DOX nanorods in NCI/RES-ADR cells was confirmed by confocal laser scanning microscopy (Fig. 3f, Fig. 3g and Fig. S12b). When free DOX was used, red fluorescence was barely observable in the cytosol; it was not concentrated in the nuclei and did not induce cytotoxicity. In contrast, after NCI/RES-ADR cells incubated with NDcc/DOX nanorods for 8 hours, red fluorescence had partly and effectively entered the nuclei, which was pink (Fig. 3f and 3g: yellow arrows). This meant that DOX molecules had been delivered to the target, leading to concrete anticancer activity. These data suggested that NDcc/DOX nanorods could be internalized by drug-resistant and drug-sensitive cancer cells.

Next, NCI/RES-ADR cells were used in the study of subcellular localization, which showed that DOX fluorescence was partly co-localized with lysosomes. This was expected due to NDcc/DOX nanorods' propensity to uptake via endocytosis processes. As shown in Fig. S13, DOX red fluorescence was also observable in the cytosol, indicating that DOX escaped from the lysosomes and was successfully delivered to the cytoplasm. We attributed this to the acidic environment of lysosomes. Due to the previously

demonstrated acid- and reduction-responsiveness of NDcc/DOX nanorods, drug release may be promoted when it enters cells mainly via endocytosis. Additionally, the red fluorescence of free DOX was barely observable in the cytosol, and there was no co-localization with lysosomes. Collectively, these results further confirmed the significantly enhanced antitumor potency of NDcc/DOX nanorods in NCI/RES-ADR cells via increased intra-cellular drug delivery and drug-DNA interactions.

Together, these results clearly demonstrated that NDcc/DOX nanorods were much more effective than free DOX in enhancing anti-proliferation efficiency in DOX-resistant NCI/RES-ADR cells, ultimately leading to apoptosis-induced anticancer activity (Fig. S14).

NDcc/DOX nanorods overcame DOX resistance of NCI/RES-ADR cancer cells due to their superior transport capactiy. This encouraged us to evaluate their hemolytic toxicity for future therapeutic applications. Neither the template **T**, the building block **BB** nor the 8mer caused any noteworthy hemolytic toxicity at low
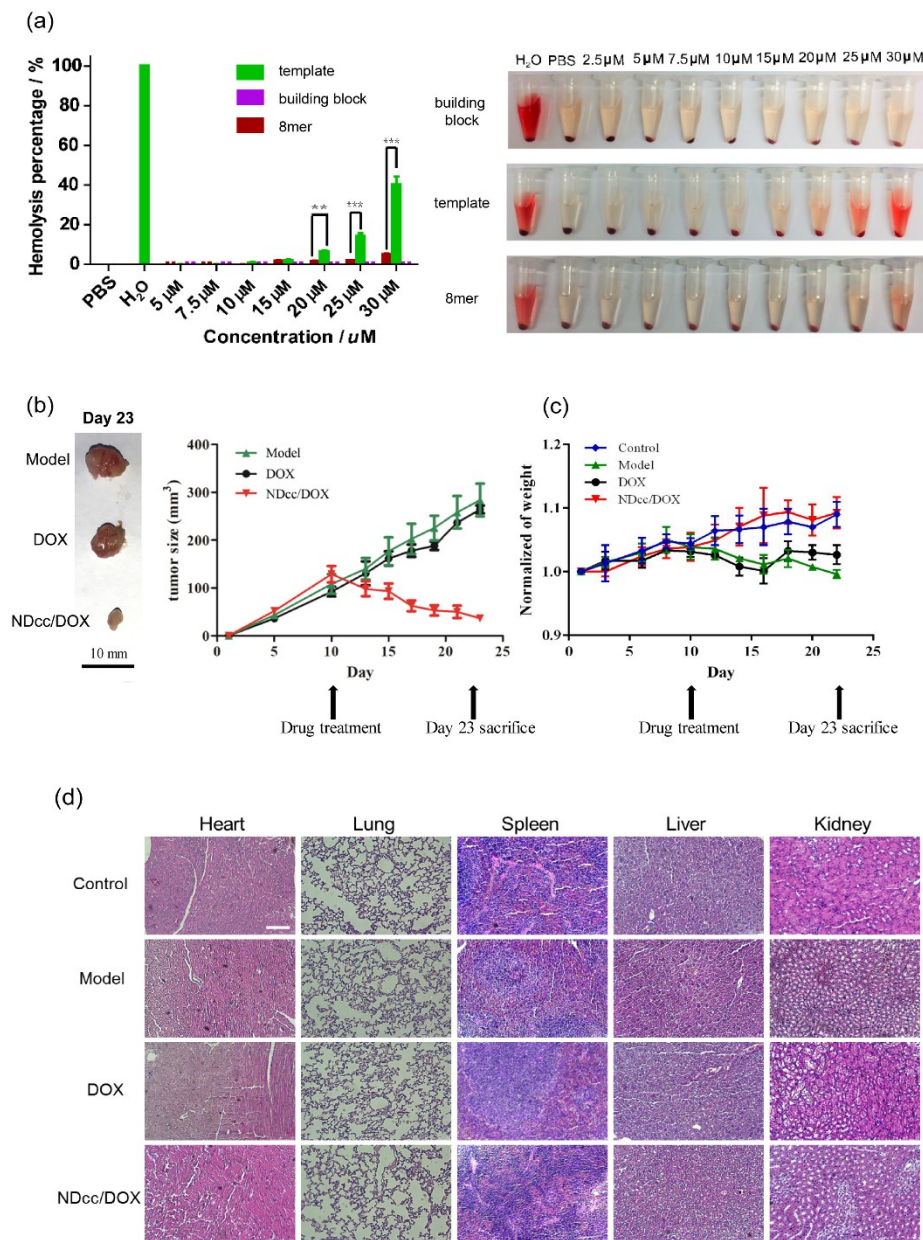

Figure 4. NDcc nanorods enhanced the DOX delivery *in vivo* with marginal effect on cardiovascular and blood hemolysis. (a) No hemolytic effect was observed with red blood cells after treated with the 8mer at varying concentrations from 2.5 to 30 μM, using water as a positive control and PBS buffer as a negative control. (b) Visualized tumor size and tumor growth curves after treating PBS (model), DOX and NDcc-DOX. (c) Animal body weight changes of the control, model, DOX, and NDcc-DOX group (control group: mice without implanted tumors). (d) H&E staining of major organs which were collected on Day 23. Scale bar, 100 μm.

concentrations (no higher than 10 μM). At higher concentrations, the 8mer still had good blood compatibility, as its hemolysis rate was 4.87% when its concentration was 30 μM. However, the template **T** (30 μM) presented obvious hemolytic toxicity with a hemolysis rate of 39.94% (Fig. 4a). These findings indicated that the hemolytic toxicity of the template **T** could be remarkably reduced by the 8mer and NDcc/DOX nanorods should be safe enough for further anti-tumour evaluation *in vivo*.

The anti-tumour effect of NDcc/DOX was further confirmed and clarified by a study of the NCI/RES-ADR xenografts model. NCI/RES-ADR cells were injected into the right armpit of BALB/c-nu mice (n=6). Mice were treated four times with DOX, NDcc/DOX and PBS buffer separately from day 10, and their body weight and the volume of tumour were measured every 2 days. As Fig. 4b shows, free DOX treatment did not inhibit tumour growth in comparison to the effect of treatment in the model group (tumour animals only treated normal saline). However, NDcc/DOX significantly enhanced anti-cancer efficacy (P<0.05). In the nanorod group, the average volume of tumours was 0.38±0.17 times that of tumours in the model group, and two tumours disappeared. In addition, in the model group and the group treated only with DOX, animals showed a small amount of body weight loss. In comparison, the weight of mice in NDcc/DOX group was very similar to that in the control group comprising mice without implanted tumours, which increased slightly since the drug treatment day (Fig. 4c).

We investigated the systemic toxicity of NDcc/DOX towards cancer cells in BALB/c-nu mice (n=6) using hematoxylin and eosin (H&E) stain. We found a minor elevation of leukocyte infiltration in the alveolar areas of the lung in the group treated only with free DOX. In the heart, the arrangement of myocardial fibres in the vertical and horizontal lines became disordered and even disappeared, which was likely due to the well-known cardiotoxicity of DOX. In comparison, the hearts of mice in the NDcc/DOX group showed clear and well-dispersed cardiomyocytes, indicating that NDcc/DOX likely reduced the toxicity of DOX. No pathological changes were observed in any other organs (Fig. 4d).

Conclusions

In summary, we employed DCC to explore a self-synthesizing nanomaterial for anti-tumour drug delivery. This strategy has been demonstrated by an example of a thiol-disulfide exchange based DCL. Under the direction of a pyridinium cation template **T** and a hydrophobic drug molecule DOX, a classical dithiol building block **BB** with a carboxylic acid group was quantitatively oxidized into a disulfide-linked macrocycle 8mer. Generally, large-sized macrocycles are entropy unfavourable. Thus, the 3mer and 4mer predominated in a library prepared only from the **BB**. Unexpectedly, macrocycles increased in size to 8mer under thermodynamic control. Two molecules of the template **T** were inclusive in the hydrophobic cavity of the 8mer with the formation of an amphiphilic complex. The complex could further self-assemble into nanorods with the encapsulation of DOX in their hydrophobic domains. Such down-hill self-assembly could shift the

equilibrium and be beneficial for the synthesis of 8mer, maximizing the DOX loading content to 40.1% of the resulting nanorods. As the self-assembly directed the synthesis of the right self-assembling molecules, the two steps were integrated into a single step. Thus, this self-synthesizing strategy was a convenient and cost-effective way to explore ideal nanorods for drug delivery. The loaded drug could be preferentially released by dual-stimuli (acid and GSH) responsiveness *in vitro* at conditions like those found at tumour lesions. Compared with free DOX, nanorods showed rapid and effective intracellular delivery of DOX. The thermodynamically oriented self-synthesizing nanorods also killed DOX resistant cancer cells. The powerful ability of nanorods to fight drug-resistance cancer was further confirmed *in vitro* and *in vivo*. Given these encouraging results, we believe that a systems chemistry-based strategy may be a promising tool for spatiotemporal control of drug delivery *in vivo*, eventually becoming a therapeutic entity in cancer treatment.

[1]   a) A. Kakkar, G. Traverso, O.C. Farokhzad, R. Weissleder, R. Langer, *Nat. Rev. Chem.* **2017**, *1*, 0063; b) J.A. Hubbell, A. Chilkoti, *Science* **2012**, *337*, 303-305.

[2]   X. Ma, Y. Zhao, *Chem. Rev.* **2015**, *115*, 7794-7839.

[3]   a) Y. Matsumura, H. Maeda, *Cancer Res.* **1986**, *46*, 6387-6392; b) V.P. Chauhan, R.K. Jain, *Nature Mater.* **2013**, *12*, 958-962.

[4]   a) K. Westesen, H. Bunjes, M. H. J. Koch, *J. Control. Release* **1997**, *48*, 223-236; b) H. Cabral, Y. Matsumoto, K. Mizuno, Q. Chen, M. Murakami, M. Kimura, Y. Terada, M. R. Kano, K. Miyazono, M. Uesaka, N. Nishiyama, K. Kataoka, *Nat. Nanotechol.* **2011**, *6*, 815-823.

[5]   a) G. Gregoriadis, *New Engl. J. Med.* **1976**, *295*, 704-710; b) H.-Y. Tung, B.-M. Chen, P.-A. Burnouf, W.-C. Huang, K.-H. Chuang, Y.-T. Yan, T.-L. Cheng, S.R. Roffler, *Mol.Cancer Ther.* **2015**, *14*, 1317-1326; c) V.P. Torchilin, *Nat. Rev. Drug Discov.* **2005**, *4*, 145-160.

[6]   a) I.I.I.T.H. Epps, R.K. O'Reilly, *Chem. Sci.* **2016**, *7*, 1674-1689; b) Y. Du, W. Chen, M. Zheng, F. Meng, Z. Zhong, *Biomaterials* **2012**, *33*, 7291-7299; c) K.A. Günay, P. Theato, H.-A. Klok, *J. Polym. Sci. Pol. Chem.* **2013**, *51*, 1-28; d) E. Randarova, H. Nakamura, R. Islam, M. Studenovsky, H. Mamoru, J. Fang, P. Chytil, T. Etrych, *Acta Biomater.* **2020**, *106*, 256-266.

[7]   a) R. Esfand, D.A. Tomalia, *Drug Discov. Today* **2001**, *6*, 427-436; b) L.

Cai, G. Xu, C. Shi, D. Guo, X. Wang, J. Luo, *Biomaterials* **2015**, *37*, 456-468; c) T. Wei, C. Chen, J. Liu, C. Liu, P. Posocco, X. Liu, Q. Cheng, S. Huo, Z. Liang, M. Fermeglia, S. Pricl, X.-J. Liang, P. Rocchi, L. Peng, *Proc. Natl Acad. Sci. USA* **2015**, *112*, 2978-2983; d) R.M. England, J.I. Moss, A. Gunnarsson, J.S. Parker, M.B. Ashford, *Biomacromolecules.* **2020**, DOI:10.1021/acs.biomac.0c00768.

[8] a) Y. Barenholz, *J. Control. Release* **2012**, *160*, 117-134; b) T. Tejada-Berges, C.O. Granai, M. Gordinier, W. Gajewski, *Expert Rev. Anticanc.* **2002**, *2*, 143-150; c) A. Sparreboom, C.D. Scripture, V. Trieu, P.J. Williams, T. De, A. Yang, B. Beals, W.D. Figg, M. Hawkins, N. Desai, *Clin. Cancer Res.* **2005**, *11*, 4136-4143; d) R.K. Jain, T. Stylianopoulos, *Nat. Rev. Clin.Oncol.* **2010**, *7*, 653-664.

[9] a) P. Huang, D. Wang, Y. Su, W. Huang, Y. Zhou, D. Cui, X. Zhu, D. Yan, *J. Am. Chem. Soc.* **2014**, *136*, 11748-11756; b) A. G. Cheetham, R. W. Chakroun, W. Ma, H. Cui, *Chem. Soc. Rev.* **2017**, *46,* 6638-6663; c) Z. Wang, J. Chen, N. Little, J. Liu, *Acta Biomater.* **2020**, *319*, 311-321.

[10] a) D. G. Waller, C. F. George, *Br. J. Pharmac.* **1989**, *28,* 497-507; b) J. Hammerstein, *Am. J. Obstet. Gynecol.* **1990**, *163*, 2198-2203; c) J. B. Zawilska, J. Wojcieszak, A. B. Olejniczak, *Pharmacol. Rep.* **2013**, *65*, 1-14.

[11] M. Kreitman, H. Akashi, *Annu. Rev. Ecol. Syst.* **1995**, *26*, 403-422.

[12] a) C. Chen, J. Tan, M. Hsieh, *Nat. Chem.* **2017**, *9*, 799–804; b) C. Pappas, R. Shafi, I. Sasselli, H. Siccardi, T. Wang, V. Narang, R. Abzalimov, N. Wijerathne, R.V. Ulijn, *Nat. Nanotechnol.* **2016**, *11*, 960–967; c) C. Reţe, N. Giuseppone, *Chem.* **2016**, *1*, 826–829; d) J. Nitschke, *Nature* **2009**, *462*, 736–738; e) A. Herrmann, *Chem. Soc. Rev.* **2014**, *43*, 1899-1933; f) J. Li, P. Nowak, S. Otto, *J. Am. Chem. Soc.* **2013**, *135*, 9222-9239; g) J.-M. Lehn, *Chem. Soc. Rev.* **2007**, *36*, 151-160; h) E. Mattia, S. Otto, *Nat. Nanotechnol.* **2015**, *10*, 111-119; i) G. Ashkenasy, T.M. Hermans, S. Otto, A.F. Taylor, *Chem. Soc. Rev.* **2017**, *46*, 2543-2554; j) C. Jia, D. Qi, Y. Zhang, K. Rissanen, J. Li, *ChemSystemsChem* **2020**, *2*, e2000019.

[13] a) L. Vial, R.F. Ludlow, J. Leclaire, R. Pérez-Fernández, S. Otto, *J. Am. Chem. Soc.* **2006**, *128*, 10253-10257; b) M. Mondal, N. Radeva, H. Fanlo-Virgós, S. Otto, G. Klebe, A.K.H. Hirsch, *Angew. Chem. Int. Ed.* **2016**, *55*, 9422–9426; *Angew. Chem.* **2016**, *128*, 9569-9574;; c) M. Lafuente, J. Solà, I. Alfonso, *Angew. Chem. Int. Ed.* **2018**, *57*, 8421–8424; d) D. Carbajo, Y. Pérez, J. Bujons, I. Alfonso, *Angew. Chem. Int. Ed.* **2020**, *59*, DOI: org/10.1002/anie.202004745; *Angew. Chem.* **2020**, *132*, DOI: org/10.1002/ange.202004745; e) H. Zhu, H. Wang, B. Shi, L.

Shangguan, W. Tong, G. Yu, Z. Mao, F. Huang, *Nat. Commun.* **2019**, *10*, 2412; f) H. Zhu, Q. Li, B. Shi, F. Ge, Y. Liu, Z. Mao, H. Zhu, S. Wang, G. Yu, F. Huang, P.J. Stang, *Angew. Chem. Int. Ed.* **2020**, *59*, DOI: 10.1002/anie.202009442.

[14] a) R.T.S. Lam, A. Belenguer, S.L. Roberts, C. Naumann, T. Jarrosson, S. Otto, J.K.M. Sanders, *Science* **2005**, *308*, 667-669; b) J. Li, P. Nowak, H. Fanlo- Virgós, S. Otto, *Chem. Sci.* **2014**, *5*, 4968-4974; c) F.B.L. Cougnon, K. Caprice, M. Pupier, A. Bauza, A. Frontera, *J. Am. Chem. Soc.* **2018**, *140*, 12442-12450; d) T. M. Gianga, G. D. Pantoș, *Nat. Commun.* **2020**, *11*, 3528.

[15] a) P. Dydio, P.A.R. Breuil, J.N.H. Reek, *Isr. J. Chem.* **2013**, *53*, 61-74; b) Z.J. Wang, K.N. Clary, R.G. Bergman, K.N. Raymond, F.D. Toste, *Nat. Chem.* **2013**, *5*, 100−103; c) H. Fanlo-Virgós, A.N.R. Alba, S. Hamieh, M. Colomb-Delsuc, S. Otto, *Angew. Chem. Int. Ed.* **2014**, *53*, 11346–11350.

[16] a) J.M.A. Carnall, C.A. Waudby, A.M. Belenguer, M.C.A. Stuart, J.J.-P. Peyralans, S. Otto, *Science* **2010**, *327*, 1502-1506; b) S. Xu, N. Giuseppone, *J. Am. Chem. Soc.* **2008**, *130*, 1826–1827; c) P. Adamski, M. Eleveld, A. Sood, Á. Kun, A. Szilágyi, T. Czárán, E. Szathmáry, S. Otto, *Nat. Rev. Chem.* **2020**, doi:10.1038/s41570-020-0196-x.

[17] S. Otto, R.L.E. Furlan, J.K.M. Sanders, *Science* **2002**, *297*, 590-593.

[18] P.T. Corbett, J.K.M. Sanders, S. Otto, *Chem. – Eur. J.* **2008**, *14*, 2153-2166.

[19] S. Otto, R. L. E. Furlan, J. K. M. Sanders, *J. Am. Chem. Soc.* **2000**, *12*, 12063-12064.

[20] Fore each reduction, 30% of the disulfides was reduced by the addition of dithiothreitol (DTT). Five times of reduction were performed to give a sufficient time to the DCL to reach equilibrium.

[21] S. Mura, J. Nicolas, P. Couvreur, *Nature Mater.* **2013**, *12*, 991-1003.

[22] V.P. Torchilin, *Nat. Rev. Drug Discov.* **2014**, *13*, 813-827.

[23] E. Hinde, K. Thammasiraphop, H. T. T. Duong, J. Yeow, B. Karagoz, C. Boyer, J. Gooding, K. Gaus, *Nat. Nanotechnol.* **2017**, *12*, 81-89.

[24] W. Ke, P. Yu, J. Wang, R. Wang, C. Guo, L. Zhou, C. Li, K. Li, *Med. Oncol.* **2011**, *28*, 135-141.

[25] a) M. Dean, T. Fojo, S. Bates, *Nat. Rev. Cancer* **2005**, *5*, 275-284; b) P. Huang, D. Wang, Y. Su, W. Huang, Y. Zhou, D. Cui, X. Zhu, D. Yan, *J. Am. Chem. Soc.* **2014**, *136*, 11748-11756; c) C.F. Higgins, *Nature* **2007**, *446*, 749-757.

[26] X. Dong, C.A. Mattingly, M.T. Tseng, M.J. Cho, Y. Liu, V.R. Adams, R.J. Mumper, *Cancer Res.* **2009**, *69*, 3918-3926.

Entry for the Table of Contents
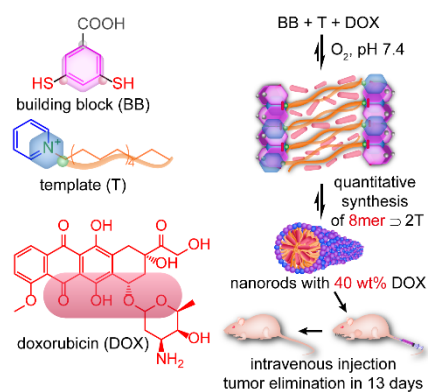
Dynamic combinatorial chemistry was employed to explore an ideal carrier molecule for anti-cancer drug delivery. Driven by thermo-dynamics, the carrier molecule was quantitatively yielded by its co-self-assembly with a template and a drug doxorubicin (DOX). The self-assembled nanocarrier with a drug-loading content of 40% was stable yet pH- and redox- responsive and could enhance drug potency and eliminate DOX-resistant cancer *in vivo* in 13 days.

Institute and/or researcher Twitter usernames: Jianwei_chem